Nature of Unconventional Pairing in the Kagome Superconductors AV_3Sb_5 ($A = K, Rb, Cs$)

Xianxin Wu,[1,2,*] Tilman Schwemmer,[3] Tobias Müller,[3] Armando Consiglio,[3] Giorgio Sangiovanni,[4] Domenico Di Sante,[5,6] Yasir Iqbal,[7] Werner Hanke,[3] Andreas P. Schnyder,[1] M. Michael Denner,[8] Mark H. Fischer,[8] Titus Neupert,[8] and Ronny Thomale[3,7,†]

[1]*Max-Planck-Institut für Festkörperforschung, Heisenbergstrasse 1, D-70569 Stuttgart, Germany*
[2]*CAS Key Laboratory of Theoretical Physics, Institute of Theoretical Physics, Chinese Academy of Sciences, Beijing 100190, China*
[3]*Institute for Theoretical Physics, University of Würzburg, Am Hubland, D-97074 Würzburg, Germany*
[4]*Institut für Theoretische Physik und Astrophysik and Würzburg-Dresden Cluster of Excellence ct.qmat, Universität Würzburg, 97074 Würzburg, Germany*
[5]*Department of Physics and Astronomy, Alma Mater Studiorum, University of Bologna, 40127 Bologna, Italy*
[6]*Center for Computational Quantum Physics, Flatiron Institute, 162 5th Avenue, New York, New York 10010, USA*
[7]*Department of Physics and Quantum Centers in Diamond and Emerging Materials (QuCenDiEM) group, Indian Institute of Technology Madras, Chennai 600036, India*
[8]*Department of Physics, University of Zurich, Winterthurerstrasse 190, 8057 Zurich, Switzerland*

(Received 1 June 2021; revised 29 July 2021; accepted 2 September 2021; published 19 October 2021)

The recent discovery of AV_3Sb_5 ($A = K, Rb, Cs$) has uncovered an intriguing arena for exotic Fermi surface instabilities in a kagome metal. Among them, superconductivity is found in the vicinity of multiple van Hove singularities, exhibiting indications of unconventional pairing. We show that the sublattice interference mechanism is central to understanding the formation of superconductivity in a kagome metal. Starting from an appropriately chosen minimal tight-binding model with multiple van Hove singularities close to the Fermi level for AV_3Sb_5, we provide a random phase approximation analysis of superconducting instabilities. Nonlocal Coulomb repulsion, the sublattice profile of the van Hove bands, and the interaction strength turn out to be the crucial parameters to determine the preferred pairing symmetry. Implications for potentially topological surface states are discussed, along with a proposal for additional measurements to pin down the nature of superconductivity in AV_3Sb_5.

DOI: 10.1103/PhysRevLett.127.177001

Introduction.—The kagome lattice has become a paradigmatic setting for exotic quantum phenomena of electronic matter. This particularly applies to quantum magnetism, where the large geometric spin frustration inherent to the corner-sharing triangles promotes the emergence of extraordinary quantum phases [1]. From an itinerant limit, electronic kagome bands are likewise particular, as they feature a flat band, Dirac cones, and van Hove singularities at different fillings. The kagome flat band suggests itself as a natural host for the realization of ferromagnetism [2,3] or possibly nontrivial topology [4–7], while the kagome Dirac cones have been proposed to be a promising way to accomplish strongly correlated Dirac fermions [8] and turbulent hydrodynamic electronic flow [9]. The kagome lattice at van Hove filling has been shown to be preeminently suited for the emergence of exotic Fermi surface instabilities [10–13]. Among others, this involves charge and spin density-wave orders with finite relative angular momentum [14]. Moreover, the kagome Hubbard model was first predicted to yield degenerate nematic instabilities which can break point-group and time-reversal symmetry simultaneously [13], which has currently regained attention in the context of twisted bilayer graphene [15].

The recent discovery of AV_3Sb_5 [16] provides an instance of kagome metals tuned to the vicinity of multiple van Hove singularities. What further makes them unique is the combination of metallicity, strong two-dimensional electronic character, and significant electronic correlations derived from the d-orbital structure of the vanadium kagome net. KV_3Sb_5 was discovered to be a kagome superconductor with $T_c = 0.93$ K [17], along with RbV_3Sb_5 ($T_c = 0.92$ K) [18] and CsV_3Sb_5 ($T_c = 2.5$ K) [19,20], where the latter was shown to rise up to $T_c = 8$ K under 2 GPa hydrostatic pressure [21–23]. While the wheel

Published by the American Physical Society under the terms of the Creative Commons Attribution 4.0 International license. Further distribution of this work must maintain attribution to the author(s) and the published article's title, journal citation, and DOI. Open access publication funded by the Max Planck Society.

of experimental exploration is still in spin, certain tendencies about the superconducting phase are starting to crystallize. The observed charge density wave (CDW) order [24], interpreted as a potential parent state for unconventional superconducting order [13,25–27], exhibits indications for an electronically driven formation [28]. Specific-heat measurements suggest at least a strongly anisotropic gap [17]. While a significant residual term from thermal conductivity suggests a nodal gap [29], penetration depth measurements claim a nodeless gap [30]. The dome shape suggests unconventional superconductivity along with a large value of $2\Delta/k_B T_c$, hinting at a strong-coupling superconductor [31].

In this Letter, we formulate a theory of unconventional superconductivity in AV_3Sb_5. In a first step, we develop an effective tight-binding model suitable for the analysis of pairing instabilities. In order to retain the necessary complexity of multiple van Hove singularities in the vicinity of the Fermi level in AV_3Sb_5, we distill a six-band minimal model. In a second step, we specify the interaction Hamiltonian. Because of matrix elements implied by the sublattice interference mechanism [11], which we review below, it is essential to take nonlocal Coulomb repulsion into consideration. Over a large range of coupling strengths, we find dominant f-wave triplet superconducting order, succeeded by d-wave singlet pairing for stronger coupling. Throughout the phase diagram, the p-wave order stays subdominant but competitive. Aside from this general trend, the detailed competition between the different orders is crucially influenced by the location of the Fermi level with respect to the multiple van Hove singularities and the nearest-neighbor (NN) Coulomb repulsion.

Sublattice decoration of kagome van Hove points.—As opposed to related hexagonal van Hove singularities such as for the bipartite honeycomb lattice, the kagome bands can host two different types of van Hove singularities which we label as sublattice mixing (m type) and sublattice pure (p type), characterized by odd and even parity at the M point, respectively. This is illustrated in Fig. 1 for the minimal kagome tight-binding model with three distinct sublattice sites located on the $3f$ Wyckoff positions of the $P6/mmm$ space group. The upper van Hove singularity ($E = 0$) is of p type, since the Fermi level eigenstates in the vicinity of the three M points are localized on mutually different sublattices (left inset). By contrast, the lower van Hove filling ($E = -2t$) has mixed sublattice character and thus is of m type, with the eigenstates equally distributed over mutually different sets of two sublattices for each M point (right inset). These distinct sublattice decorations have a strong impact on the nesting properties [see Sec. II of Supplemental Material (SM) [32]]. Since p-type van Hove points do not couple to each other via local interactions, the inclusion of at least NN Coulomb repulsion is quintessential to adequately model interacting kagome metals close to p-type van Hove filling [11,39].

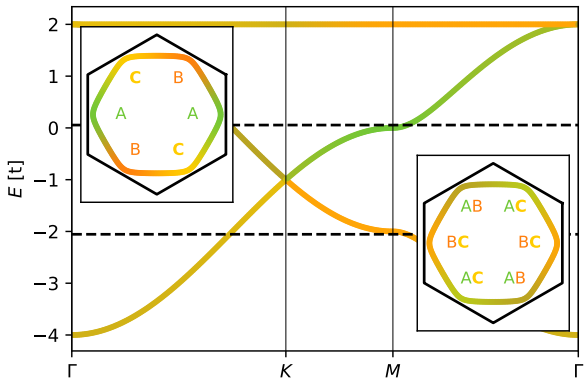

FIG. 1. Generic three-band kagome dispersion exhibits two van Hove singularities with distinct sublattice (A, B, C) decoration. Whereas the upper van Hove filling at $E = 0$ has a pure sublattice makeup (p type, left inset), the lower van Hove filling at $E = -2t$ mixes different sublattice states (m type, right inset). Energy is measured in units of the NN hybridization t.

Effective model.—The *ab initio* band structure of AV_3Sb_5 matches well with angle-resolved photoemission spectroscopy (ARPES) measurements below the CDW transition temperature, even though the corresponding density functional theory calculations are performed neglecting the star-of-David-type structural distortion [19,40]. Because of the multiple sublattices and the large number of contributing orbitals from both V and Sb in the vicinity of the Fermi level, a reduction to an effective model is a prerequisite to any analysis of many-body instabilities.

The layered structure of AV_3Sb_5, together with the large transport anisotropy of $\rho_c/\rho_{ab} \approx 600$ [19] (for CsV_3Sb_5) allows us to constrain ourselves to the two-dimensional V-Sb kagome plane. Analyzing the Fermi level at $k_z = 0$ by means of density functional theory, we find three distinct Fermi surfaces in AV_3Sb_5: (i) a pocket composed of vanadium d_{xy}, $d_{x^2-y^2}$, d_{z^2} orbitals in proximity to a p-type van Hove singularity, (ii) two additional pockets composed of vanadium d_{xz}, d_{yz} orbitals in proximity to another p-type and m-type van Hove singularity above and below the Fermi level, respectively (Fig. 2), and (iii) a circular pocket around Γ formed by antimony p_z orbitals. Note that (i) and (ii) do not hybridize due to opposite M_z eigenvalues and the symmetrywise allowed hybridization of (ii) and (iii) is parametrically weak. These features are not particularly sensitive to spin-orbit coupling, which is hence not further considered in the following.

For the effective model, we restrict ourselves to the Fermi pockets (ii) for three reasons. First, the pockets in (ii) carry the dominant density of states at the Fermi level. Second, we preserve the complexity of multiple van Hove singularities of p type and m type in our minimal model. Third, upon comparison to the *ab initio* band structure, our minimal model manages to correctly capture all irreducible band representations at the high symmetry points in the Brillouin zone. The constituting $d_{xz/yz}$ orbitals belong to

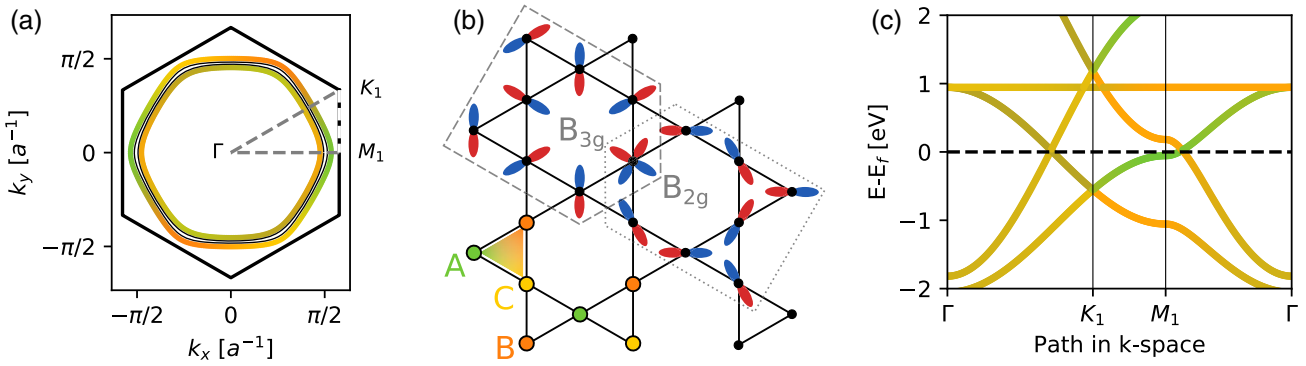

FIG. 2. (a) Fermi surfaces of the minimal two-orbital tight-binding model [Eq. (1)] for a vanadium kagome net. Both a p-type and m-type van Hove filling are present nearby the Fermi level, indicated by their respective orbital color. (b) Real-space structure of the kagome V planes. The sign structure (blue or red) and spatial orientation of the B_{2g} and B_{3g} orbitals is sketched on different lattice sites. The red, yellow, and orange coloring indicates the three kagome sublattices. (c) Band structure along the high-symmetry path depicted by the dashed line in (a). The band coloring indicates the sublattice support of the momentum eigenstates.

the $B_{2g/3g}$ irreducible representations of the site symmetry group D_{2h} for the $3f$ Wyckoff positions [Fig. 2(b)], forming a set of bands with opposite mirror eigenvalues along the Γ-M line. These bands give rise to a mirror-symmetry-protected Dirac cone on the Γ-M line and hence, an upper and lower van Hove filling with opposite sublattice parity (Fig. 2). Employing the D_{6h} point-group symmetry, our corresponding effective six-band Hamiltonian can then be derived as

$$H = \sum_{\mathbf{k}i\alpha} \epsilon_\alpha c^\dagger_{\mathbf{k}i\alpha} c_{\mathbf{k}i\alpha} - \sum_{\mathbf{k}ij\alpha} t_\alpha \Phi_{ij}(\mathbf{k}) c^\dagger_{\mathbf{k}j\alpha} c_{\mathbf{k}i\alpha} - t' \sum_{\mathbf{k},ij} \Phi_{ij}(\mathbf{k}) s_{ij} (c^\dagger_{\mathbf{k}jxz} c_{\mathbf{k}iyz} - c^\dagger_{\mathbf{k}jyz} c_{\mathbf{k}ixz}), \quad (1)$$

where ($i = A, B, C$ and $\alpha = xz, yz$). The crystal field splitting is denoted by ϵ_α, where the operator $c^\dagger_{\mathbf{k}i\alpha}$ ($c_{\mathbf{k}i\alpha}$) creates (annihilates) an electron with momentum $\mathbf{k}$ of sublattice i in orbital α. The lattice structure factors read $\Phi_{AB}(\mathbf{k}) = 1 + e^{-2i\mathbf{k}\cdot\mathbf{a}_1}$, $\Phi_{BC}(\mathbf{k}) = 1 + e^{-2i\mathbf{k}\cdot\mathbf{a}_3}$, and $\Phi_{AC}(\mathbf{k}) = 1 + e^{-2i\mathbf{k}\cdot\mathbf{a}_2}$ obeying the Hermiticity condition $\Phi_{ij}(\mathbf{k}) = (1 - \delta_{ij})\Phi^*_{ji}(\mathbf{k})$, where the sublattice-connecting vectors are denoted by $\mathbf{a}_{1,2} = (\sqrt{3}/2, \pm 1/2)^T$ and $\mathbf{a}_3 = (0, -1)^T$. The second term represents the intraorbital NN hoppings on the kagome lattice with two distinct amplitudes t_α, while the third term describes NN interorbital hopping amplitude t'. The nontrivial transformation properties of the d_{xz} and d_{yz} orbitals under the site-symmetry group result in a nontrivial sign structure for the third term, described by $s_{AC} = s_{CB} = -s_{AB}$ and $s_{ij} = -s_{ji}$. We approximately fit our model to the *ab initio* band structure (see Sec. IV of SM) and obtain the parameters $t_{xz} = 1$ eV, $t_{yz} = 0.5$ eV, $t' = 0.002$ eV, $\epsilon_{xz} = 2.182$ eV, and $\epsilon_{yz} = -0.055$ eV. The corresponding band structure and Fermi surfaces are shown in Fig. 2.

RPA analysis.—For the electronic interactions, we consider multiorbital density-density type interactions up to NNs

$$H_{\text{int}} = U \sum_{li\alpha} n_{li\alpha\uparrow} n_{li\alpha\downarrow} + U' \sum_{li,\alpha<\beta} n_{li\alpha} n_{li\beta} + J \sum_{li,\alpha<\beta,\sigma\sigma'} c^\dagger_{li\alpha\sigma} c^\dagger_{li\beta\sigma'} c_{li\alpha\sigma'} c_{li\beta\sigma} + J' \sum_{li,\alpha\neq\beta} c^\dagger_{li\alpha\uparrow} c^\dagger_{li\alpha\downarrow} c_{li\beta\downarrow} c_{li\beta\uparrow} + \sum_{\langle ll'\rangle ij\alpha\beta} V_{\alpha\beta} n_{li\alpha} n_{l'j\beta}, \quad (2)$$

where $n_{li\alpha} = n_{li\alpha\uparrow} + n_{li\alpha\downarrow}$ and l, l' is an index for the unit cell. U, U', J, and J' denote the on-site intraorbital, interorbital repulsion, Hund's coupling, and pair-hopping terms, respectively. $V_{\alpha\beta}$ denotes the repulsion between NN sites. In the following we adopt the parametrization $U = U' + 2J$, $J = J'$ with $J = 0.1U$ and $V_{\alpha\beta} = 0.3U \;\; \forall\, \alpha, \beta$ consistent with our *ab initio* constrained random-phase approximation estimates for a target manifold comprising V-3d and Sb-5p orbitals [41]. An extensive *ab initio* study of interactions and their dependence on the effective low-energy model will be presented elsewhere.

The inset of Fig. 3 displays the leading eigenvalue of the bare susceptibility $\chi_0(\boldsymbol{q})$ along high-symmetry lines. It is mainly attributed to the d_{yz} orbital and features three prominent peaks. The largest two are located proximate to the Γ point, while the peak close to M is suppressed through sublattice interference. Including on-site and NN interactions at the RPA level, these peaks get significantly enhanced in the spin as well as charge channel. Note that, indeed, we find the charge susceptibility at the verge of diverging around the M point for strong NN repulsion, hinting at an incident CDW instability.

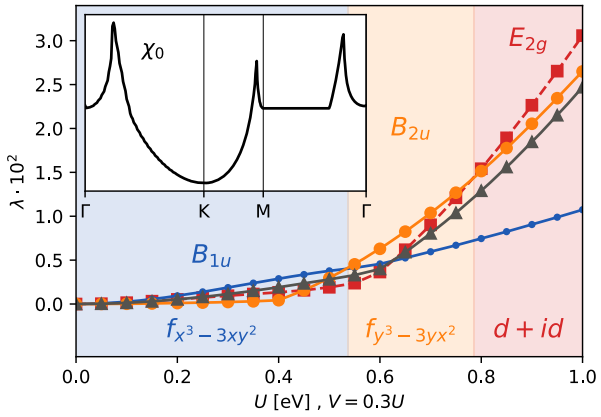

FIG. 3. Pairing-strength eigenvalues λ for the dominant instabilities as a function of U ($V = 0.3U$, $J = 0.1U$) in Eq. (2). Continuous (dashed) lines indicate triplet (singlet) pairing. Two distinct f-wave solutions, B_{1u} (blue dots) and B_{2u} (large orange dots), dominate for smaller interaction scales. The d-wave E_{2g} solution dominates for larger U. The p-wave E_{2u} solution (gray triangles) is subleading, but competitive at all U. The upper left inset depicts the largest eigenvalue trajectory of the bare susceptibility $\chi_0(\boldsymbol{q})$ along the high-symmetry path indicated in Fig. 2(a).

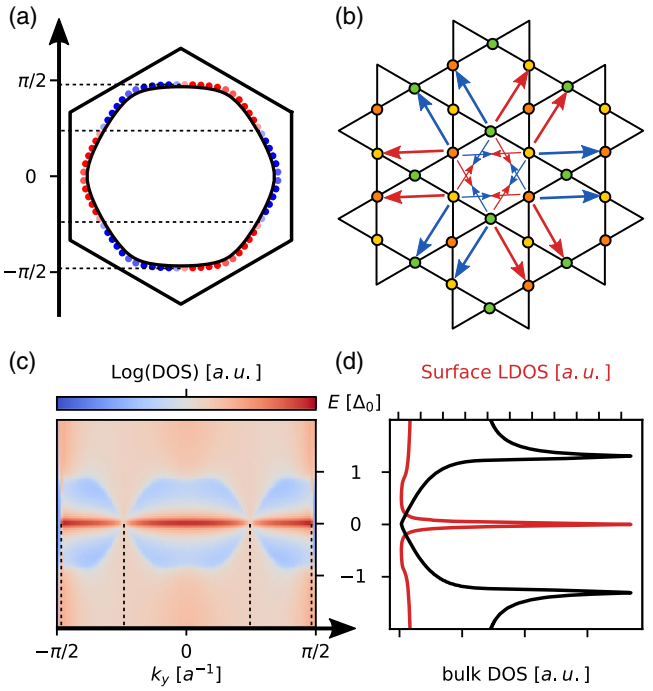

FIG. 4. The intersublattice triplet $f_{x^3-3xy^2}$-wave pairing function in (a) momentum and (b) real space, where the superconducting order parameter changes sign under 60° rotation. (c) Edge spectra for open boundary conditions along x direction; zero-energy Andreev bound states appear between the projections of nodal points in the f-wave pairing. (d) Density of states for the bulk f-wave pairing (black) and local density of states at edges from Andreev bound states (red).

Below the critical interaction, superconductivity emerges, triggered by charge and spin fluctuations [42–44]. The obtained pairing eigenvalues as a function of U are displayed in Fig. 3. For $U < 0.54$ eV, pairing on the p-type Fermi sheet from the p-type van Hove band with B_{1u} ($f_{x^3-3xy^2}$-wave) symmetry is favored and E_{1u} (p-wave) and E_{2g} (d-wave) pairings are subdominant. Increasing the coupling results in a rapid increase of the B_{2u} ($f_{y^3-3yx^2}$ wave) and E_{2g} pairings on the Fermi sheet from the m-type van Hove band, where the spin-triplet solution still dominates slightly. Upon further increase of the interaction strength, the d-wave pairing on this Fermi sheet becomes dominant. Meanwhile, the E_{1u} pairing is subdominant. Varying the ratio of V/U ($0.2 < V/U < 0.35$) does not qualitatively change the above results in the six-band tight-binding model (see Sec. IV of SM [32]). Note that we have also performed calculations with a seven-band tight-binding model including the circular pocket around Γ [45] and find that it has negligible effect on the pairing (see Sec. IV of SM [32]).

We further analyze the harmonic fingerprint of the obtained pairings. The $f_{x^3-3xy^2}$-wave pairing is dominated by the sublattice-pure d_{yz} Fermi surface and the corresponding gap function in k space is shown in Fig. 4(a), where there are line nodes along Γ-K and the superconducting gap changes sign under 60° rotation. The corresponding real-space pairing is displayed in Fig. 4(b), which represents a spin-triplet sublattice-triplet pairing between d_{yz} orbitals on the next-nearest-neighbor (NNN) sites. This pairing is promoted by the effective interaction between the NNN sites from the second-order effect of NN repulsion, an effect which is robust to including diagrams beyond the RPA approximation as one would do in a functional renormalization group study [46,47]. Counterintuitively, we find that both B_{2u} and E_{2g} states, favored at larger V, are dominated by the sublattice-mixing d_{xz} Fermi surface and attributed to the pairing between d_{xz} orbitals on the NN sites. The B_{2u} pairing, different from the B_{1u} pairing, possesses line nodes along the Γ-M direction. We expect the twofold degenerate E_{2g} pairing instability to form a $d+id$ state below T_c in order to maximize condensation energy, which spontaneously breaks time-reversal symmetry. Notably, as a particular feature of the kagome lattice, the pairings between NN sites are promoted by the interorbital NN repulsion: although there is a direct repulsion between the NN sublattices, the second-order contribution via the other sublattices can be attractive. Once it overcomes the direct repulsion term, the effective interaction between NN sites becomes attractive and can promote NN pairing. Furthermore, note that the superconducting gap in the obtained states for our minimal model are either dominant on the d_{yz} or d_{xz} Fermi surface, which can be attributed to the assumed weak interorbital hopping.

Topological properties of the pairing states.—Our minimal-model analysis is dominated by an f-wave state for weak coupling. Combined with the observation that the band renormalization in ARPES appears moderate, f-wave order could be a favored candidate for the nature of pairing in AV_3Sb_5. For time-reversal-invariant superconductors, the topological criterion about zero-energy Andreev bound states on edges is determined by winding numbers [48,49]. For both f-wave pairing states emerging in our analysis, each node carries a winding number of $+1$ or -1. If we impose open boundary conditions, where the projections of nodes with opposite winding number do not overlap, a zero-energy flat band connecting the projections of nodes is created. For illustration, we present the surface spectrum of the $f_{x^3-3xy^2}$-wave state with open boundary conditions along the x direction in Fig. 4(c). The corresponding local density of states features a sharp zero-bias peak, shown in Fig. 4(d) which could be observed at corresponding step edges in STM measurements. A similar analysis can likewise be performed for the d-wave and p-wave state. Chiral superconductors, which are likely to result from either d-wave or p-wave instabilities on hexagonal lattices, are potential hosts to Majorana zero modes in their vortex cores [50,51].

Experimental signatures.—The observation of a finite κ/T for $T \to 0$ in thermal conductance measurements [29] as well as the typical V-shaped gap in STM measurements [31] have provided supporting experimental evidence for a nodal gap in AV_3Sb_5, which would be in line with f-wave pairing which we obtain in a large parameter regime for our minimal model. An f-wave state will have additional, clear experimental signatures. First, since the f-wave state pairs electrons in the spin-triplet channel, we expect the spin susceptibility in the superconducting phase to stay constant upon lowering the temperature, which should be seen in Knight-shift measurements. A further signature of spin-triplet pairing is often a high critical field. However, recent critical field measurements for both in-plane [52] and out-of-plane [29] fields indicate orbital limiting at rather low fields, such that the critical fields cannot distinguish the Cooper-pair spin structure. Finally, many thermodynamic quantities allow us to identify the nodal structure through the temperature scaling of their low-temperature behavior. With the f-wave order parameter being the only one with symmetry imposed nodes, the low-energy excitations due to these nodes can directly probe this order without requiring phase information. The to date strongest evidence for the f-wave state comes indeed from thermal conductance measurements in Ref. [29]. In order to strengthen this conclusion, other thermodynamic probes, such as the electronic specific heat, penetration depth, or $1/T_1$ in NMR should show a square, linear, and cubic temperature dependence [53], respectively. Note, however, that disorder washes out these low-energy signatures. Chiral p-wave and d-wave superconductivity would be in line with a possibly highly anisotropic, but nodeless gap. Furthermore, concomitant signatures of time-reversal symmetry breaking could be revealed through Kerr measurements, μ-SR below T_c, or even new experimental approaches such as the detection of clapping modes [54]. Most importantly, for the specific scenario of multiple van Hove singularities, the double dome feature in the superconducting phase can tentatively be understood by the evolution of the individual van Hove bands as a function of pressure [21,23].

Our work shows the unique principles for unconventional pairing in kagome metals, which promises to unlock a whole new paradigm of electronically mediated superconductivity.

This work is funded by the Deutsche Forschungsgemeinschaft (DFG, German Research Foundation) through Project-ID 258499086—SFB 1170 and through the Würzburg-Dresden Cluster of Excellence on Complexity and Topology in Quantum Matter—ct.qmat Project-ID 390858490—EXC 2147. Y. I. acknowledges financial support by the Science and Engineering Research Board (SERB), Department of Science and Technology (DST), India through the Startup Research Grant No. SRG/2019/000056 and MATRICS Grant No. MTR/2019/001042, the Abdus Salam International Centre for Theoretical Physics (ICTP) through the Simons Associateship scheme funded by the Simons Foundation, IIT Madras through the Institute of Eminence (IoE) program for establishing the QuCenDiEM group (Project No. SB20210813PHMHRD002720), and the International Centre for Theoretical Sciences (ICTS), Bengaluru, India during a visit for participating in the program "Novel phases of quantum matter" (Code: ICTS/topmatter2019/12). This research was supported in part by the National Science Foundation under Grant No. NSF PHY-1748958. This project has received funding from the European Research Council (ERC) under the European Unions Horizon 2020 research and innovation programm (ERC-StG-Neupert-757867-PARATOP). The research leading to these results has received funding from the European Unions Horizon 2020 research and innovation programme under the Marie Skłodowska-Curie Grant Agreement No. 897276. The authors gratefully acknowledge the Gauss Centre for Supercomputing e.V. [55] for funding this project by providing computing time on the GCS Supercomputer SuperMUC at Leibniz Supercomputing Centre [56]. Y. I. acknowledges the use of the computing resources at HPCE, IIT Madras.

*xianxin.wu@fkf.mpg.de
†rthomale@physik.uni-wuerzburg.de

[1] M. R. Norman, Colloquium: Herbertsmithite and the search for the quantum spin liquid, Rev. Mod. Phys. **88**, 041002 (2016).
[2] A Mielke, Ferromagnetic ground states for the Hubbard model on line graphs, J. Phys. A **24**, L73 (1991).

[3] F. Pollmann, P. Fulde, and K. Shtengel, Kinetic Ferromagnetism on a Kagome Lattice, Phys. Rev. Lett. **100**, 136404 (2008).

[4] S. A. Parameswaran, R. Roy, and S. L. Sondhi, Fractional quantum Hall physics in topological flat bands, C. R. Acad. Sci. **14**, 816 (2013).

[5] C. Hua Lee, D. P. Arovas, and R. Thomale, Band flatness optimization through complex analysis, Phys. Rev. B **93**, 155155 (2016).

[6] J.-X. Yin *et al.*, Quantum-limit Chern topological magnetism in $TbMn_6Sn_6$, Nature (London) **583**, 533 (2020).

[7] D.-S. Ma, Y. Xu, C. S. Chiu, N. Regnault, A. A. Houck, Z. Song, and B. Andrei Bernevig, Spin-Orbit-Induced Topological Flat Bands in Line and Split Graphs of Bipartite Lattices, Phys. Rev. Lett. **125**, 266403 (2020).

[8] I. I. Mazin, H. O. Jeschke, F. Lechermann, H. Lee, M. Fink, R. Thomale, and R. Valentí, Theoretical prediction of a strongly correlated Dirac metal, Nat. Commun. **5**, 4261 (2014).

[9] D. Di Sante, J. Erdmenger, M. Greiter, I. Matthaiakakis, R. Meyer, D. Rodríguez Fernández, R. Thomale, E. van Loon, and T. Wehling, Turbulent hydrodynamics in strongly correlated Kagome metals, Nat. Commun. **11**, 3997 (2020).

[10] S.-L. Yu and J.-X. Li, Chiral superconducting phase and chiral spin-density-wave phase in a Hubbard model on the kagome lattice, Phys. Rev. B **85**, 144402 (2012).

[11] M. L. Kiesel and R. Thomale, Sublattice interference in the kagome Hubbard model, Phys. Rev. B **86**, 121105(R) (2012).

[12] W.-S. Wang, Z.-Z. Li, Y.-Y. Xiang, and Q.-H. Wang, Competing electronic orders on kagome lattices at van Hove filling, Phys. Rev. B **87**, 115135 (2013).

[13] M. L. Kiesel, C. Platt, and R. Thomale, Unconventional Fermi Surface Instabilities in the Kagome Hubbard Model, Phys. Rev. Lett. **110**, 126405 (2013).

[14] C. Nayak, Density-wave states of nonzero angular momentum, Phys. Rev. B **62**, 4880 (2000).

[15] R. M. Fernandes and J. W. F. Venderbos, Nematicity with a twist: Rotational symmetry breaking in a moiré superlattice, Sci. Adv. **6**, eaba8834 (2020).

[16] B. R. Ortiz, L. C. Gomes, J. R. Morey, M. Winiarski, M. Bordelon, J. S. Mangum, I. W. H. Oswald, J. A. R.-Rivera, J. R. Neilson, S. D. Wilson, E. Ertekin, T. M. McQueen, and E. S. Toberer, New kagome prototype materials: Discovery of KV_3Sb_5, RbV_3Sb_5, and CsV_3Sb_5, Phys. Rev. Mater. **3**, 094407 (2019).

[17] B. R. Ortiz, P. M. Sarte, E. M. Kenney, M. J. Graf, S. M. L. Teicher, R. Seshadri, and S. D. Wilson, Superconductivity in the $\mathbb{Z}_2$ kagome metal KV_3Sb_5, Phys. Rev. Mater. **5**, 034801 (2021).

[18] Q. Yin, Z. Tu, C. Gong, Y. Fu, S. Yan, and H. Lei, Superconductivity and normal-state properties of kagome metal RbV_3Sb_5 single crystals, Chin. Phys. Lett. **38**, 037403 (2021).

[19] B. R. Ortiz, S. M. L. Teicher, Y. Hu, J. L. Zuo, P. M. Sarte, E. C. Schueller, A. M. Milinda Abeykoon, M. J. Krogstad, S. Rosenkranz, R. Osborn, R. Seshadri, L. Balents, J. He, and S. D. Wilson, CsV_3Sb_5: A $\mathbb{Z}_2$ Topological Kagome Metal with a Superconducting Ground State, Phys. Rev. Lett. **125**, 247002 (2020).

[20] H. Zhao, H. Li, B. R. Ortiz, S. M. L. Teicher, T. Park, M. Ye, Z. Wang, L. Balents, S. D. Wilson, and I. Zeljkovic, Cascade of correlated electron states in a kagome superconductor CsV_3Sb_5, arXiv:2103.03118.

[21] K. Y. Chen, N. N. Wang, Q. W. Yin, Z. J. Tu, C. S. Gong, J. P. Sun, H. C. Lei, Y. Uwatoko, and J.-G. Cheng, Double Superconducting Dome and Triple Enhancement of T_c in the Kagome Superconductor CsV_3Sb_5 Under High Pressure, Phys. Rev. Lett. **126**, 247001 (2021).

[22] Z. Zhang, Z. Chen, Y. Zhou, Y. Yuan, S. Wang, L. Zhang, X. Zhu, Y. Zhou, X. Chen, J. Zhou, and Z. Yang, Pressure-induced reemergence of superconductivity in topological kagome metal CsV_3Sb_5, Phys. Rev. B **103**, 224513 (2021).

[23] X. Chen, X. Zhan, X. Wang, J. Deng, X.-b. Liu, X. Chen, J.-g. Guo, and X. Chen, Highly-robust reentrant superconductivity in CsV_3Sb_5 under pressure, Chin. Phys. Lett. **38**, 057402 (2021).

[24] Y.-X. Jiang *et al.*, Discovery of unconventional chiral charge order in kagome superconductor KV_3Sb_5, Nat. Mater. **20**, 1353 (2021).

[25] X. Feng, K. Jiang, Z. Wang, and J. Hu, Chiral flux phase in the Kagome superconductor AV_3Sb_5, Sci. Bull. **66**, 1384 (2021).

[26] M. Michael Denner, R. Thomale, and T. Neupert, Analysis of charge order in the kagome metal AV_3Sb_5 (A = K, Rb, Cs), arXiv:2103.14045.

[27] Y.-P. Lin and R. M. Nandkishore, Complex charge density waves at Van Hove singularity on hexagonal lattices: Haldane-model phase diagram and potential realization in kagome metals AV_3Sb_5, Phys. Rev. B **104**, 045122 (2021).

[28] H. X. Li, T. T. Zhang, Y.-Y. Pai, C. Marvinney, A. Said, T. Yilmaz, Q. Yin, C. Gong, Z. Tu, E. Vescovo, R. G. Moore, S. Murakami, H. C. Lei, H. N. Lee, B. Lawrie, and H. Miao, Observation of Unconventional Charge Density Wave without Acoustic Phonon Anomaly in Kagome Superconductors AV_3Sb_5 (A = Rb, Cs), Phys. Rev. X **11**, 031050 (2021).

[29] C. C. Zhao, L. S. Wang, W. Xia, Q. W. Yin, J. M. Ni, Y. Y. Huang, C. P. Tu, Z. C. Tao, Z. J. Tu, C. S. Gong, H. C. Lei, Y. F. Guo, X. F. Yang, and S. Y. Li, Nodal superconductivity and superconducting domes in the topological Kagome metal CsV_3Sb_5, arXiv:2102.08356.

[30] W. Duan, Z. Nie, S. Luo, F. Yu, B. R. Ortiz, L. Yin, H. Su, F. Du, A. Wang, Y. Chen, X. Lu, J. Ying, S. D. Wilson, X. Chen, Y. Song, and H. Yuan, Nodeless superconductivity in the kagome metal CsV_3Sb_5, Sci. China-Phys. Mech. Astron. **64**, 107462 (2021).

[31] H. Chen *et al.*, Roton pair density wave and unconventional strong-coupling superconductivity in a topological kagome metal, arXiv:2103.09188.

[32] See Supplemental Material at http://link.aps.org/supplemental/10.1103/PhysRevLett.127.177001 for susceptibilities for two types of van-Hove singularities, the details about RPA calculations and pairing in real space and the comparison of the DFT with the tight-binding band structures, which includes Refs. [33–38].

[33] A. F. Kemper, T. A. Maier, S. Graser, H.-P. Cheng, P. J. Hirschfeld, and D. J. Scalapino, Sensitivity of the superconducting state and magnetic susceptibility to key aspects

of electronic structure in ferropnictides, New J. Phys. **12**, 073030 (2010).
[34] N. E. Bickers, D. J. Scalapino, and S. R. White, Conserving Approximations for Strongly Correlated Electron Systems: Bethe-Salpeter Equation and Dynamics for the Two-Dimensional Hubbard Model, Phys. Rev. Lett. **62**, 961 (1989).
[35] K. Kubo, Pairing symmetry in a two-orbital Hubbard model on a square lattice, Phys. Rev. B **75**, 224509 (2007).
[36] X. Wu, J. Yuan, Y. Liang, H. Fan, and J. Hu, g-wave pairing in BiS_2 superconductors, Europhys. Lett. **108**, 27006 (2014).
[37] X. Wu, F. Yang, C. Le, H. Fan, and J. Hu, Triplet p_z-wave pairing in quasi-one-dimensional $A_2Cr_3As_3$ superconductors $(a = \mathrm{K}, \mathrm{Rb}, \mathrm{Cs})$, Phys. Rev. B **92**, 104511 (2015).
[38] E. M. Kenney, B. R. Ortiz, C. Wang, S. D. Wilson, and M. J. Graf, Absence of local moments in the kagome metal KV_3Sb_5 as determined by muon spin spectroscopy, J. Phys. Condens. Matter **33**, 235801 (2021).
[39] J. Zhao, W. Wu, Y. Wang, and S. A. Yang, Electronic correlations in the normal state of kagome superconductor KV_3Sb_5, Phys. Rev. B **103**, L241117 (2021).
[40] H. Tan, Y. Liu, Z. Wang, and B. Yan, Charge Density Waves and Electronic Properties of Superconducting Kagome Metals, Phys. Rev. Lett. **127**, 046401 (2021).
[41] F. Aryasetiawan, M. Imada, A. Georges, G. Kotliar, S. Biermann, and A. I. Lichtenstein, Frequency-dependent local interactions and low-energy effective models from electronic structure calculations, Phys. Rev. B **70**, 195104 (2004).
[42] D. J. Scalapino, E. Loh, and J. E. Hirsch, d-wave pairing near a spin-density-wave instability, Phys. Rev. B **34**, 8190 (1986).
[43] S. Onari, R. Arita, K. Kuroki, and H. Aoki, Phase diagram of the two-dimensional extended Hubbard model: Phase transitions between different pairing symmetries when charge and spin fluctuations coexist, Phys. Rev. B **70**, 094523 (2004).
[44] S. Graser, T. A. Maier, P. J. Hirschfeld, and D. J. Scalapino, Near-degeneracy of several pairing channels in multiorbital models for the Fe pnictides, New J. Phys. **11**, 025016 (2009).
[45] H. Sakakibara, H. Usui, K. Suzuki, T. Kotani, H. Aoki, and K. Kuroki, Model Construction and a Possibility of Cuprate-like Pairing in a New d^9 Nickelate Superconductor $(\mathrm{Nd}, \mathrm{Sr})NiO_2$, Phys. Rev. Lett. **125**, 077003 (2020).
[46] C. Honerkamp, Density Waves and Cooper Pairing on the Honeycomb Lattice, Phys. Rev. Lett. **100**, 146404 (2008).
[47] X. Wu, W. Hanke, M. Fink, M. Klett, and R. Thomale, Harmonic fingerprint of unconventional superconductivity in twisted bilayer graphene, Phys. Rev. B **101**, 134517 (2020).
[48] M. Sato, Y. Tanaka, K. Yada, and T. Yokoyama, Topology of Andreev bound states with flat dispersion, Phys. Rev. B **83**, 224511 (2011).
[49] A. P. Schnyder, P. M. R. Brydon, and C. Timm, Types of topological surface states in nodal noncentrosymmetric superconductors, Phys. Rev. B **85**, 024522 (2012).
[50] D. A. Ivanov, Non-Abelian Statistics of Half-Quantum Vortices in p-Wave Superconductors, Phys. Rev. Lett. **86**, 268 (2001).
[51] M. Sato, Y. Takahashi, and S. Fujimoto, Non-Abelian topological orders and Majorana fermions in spin-singlet superconductors, Phys. Rev. B **82**, 134521 (2010).
[52] F. Du, S. Luo, B. R. Ortiz, Y. Chen, W. Duan, D. Zhang, X. Lu, S. D. Wilson, Y. Song, and H. Yuan, Pressure-tuned interplay between charge order and superconductivity in the kagome metal KV_3Sb_5, Phys. Rev. B **103**, L220504 (2021).
[53] B. Zinkl, M. H. Fischer, and M. Sigrist, Superconducting gap anisotropy and topological singularities due to lattice translational symmetry and their thermodynamic signatures, Phys. Rev. B **100**, 014519 (2019).
[54] N. R. Poniatowski, J. B. Curtis, A. Yacoby, and P. Narang, Spectroscopic signatures of time-reversal symmetry breaking superconductivity, arXiv:2103.05641.
[55] http://www.gauss-centre.eu.
[56] http://www.lrz.de.